Electric Power Systems Research 220 (2023) 109302

Contents lists available at ScienceDirect

Electric Power Systems Research

journal homepage: www.elsevier.com/locate/epsr

A single-ended traveling wave based fault location method using DWT in hybrid parallel HVAC/HVDC overhead transmission lines on the same tower

Mohammad Fayazi, Mahmood Joorabian *, Alireza Saffarian, Mehdi Monadi

Department of Electrical Engineering, Faculty of Engineering, Shahid Chamran University of Ahvaz, Ahvaz 61357-85311, Iran

ARTICLE INFO

Keywords:
Hybrid parallel HVAC/HVDC overhead transmission line
AC and DC faults
Intersystem faults
Fault location
Discrete Wavelet Transform (DWT)
Traveling wave (TW)
Signal processing

ABSTRACT

In this paper, a single ended traveling wave based fault location method is presented for Hybrid Parallel HVAC/HVDC Overhead Transmission Lines (HPOTLs) on the same tower using Discrete Wavelet Transform (DWT). In HPOTLs, the AC and DC transmission lines are adjacent to each other from the sending to the receiving end of the lines and there is electromagnetic coupling between them. Fault detection and classification algorithms in HPOTLs are presented in another paper. Therefore, in order to summarizing, in this paper, it is assumed that the fault is detected in the HVAC or/and HVDC lines and faulty line is identified. HPOTL faults include AC faults, DC faults and AC/DC intersystem faults. AC and DC voltage signals on sending end of the transmission line with a sampling frequency of 100 kHz are used for fault location in this paper. In order to minimize the noise effect, the squared wavelet transform coefficients (WTC^2) is used for proposed fault location method. Finally, Bewley-Lattice diagrams are checked for the traveling wave pattern and locate the fault. At the end of paper, it has been shown that the proposed method has high accuracy, noise immunity, robustness against fault inception angles, and high impedance faults.

1. Introduction

Nowadays, HVDC transmission lines are widely used in transmission networks due to many advantages such as higher power transmission capacity over long distances, higher reliability and lower transmission losses than HVAC transmission lines. For the reasons mentioned, in some existing transmission lines in the world, to increase the transmission capacity of HVAC transmission lines, multi-circuit AC lines are converted into hybrid parallel HVAC/HVDC transmission lines [1]. In some other cases, due to environmental reasons and reduction of transmission line Right-of-Way (ROW), AC and DC transmission lines are transferred in parallel and adjacent to each other. In all these cases, due to the proximity of AC and DC transmission lines and the induction of voltage and current components in both transmission lines, the performance of each line in different conditions affects the other line, especially its protection systems and fault location algorithms [2–4]. This effect can be caused by electromagnetic coupling or direct galvanic contact. Fault location in HPOTLs is an issue that will become more important with the growth of HPOTLs in the transmission network.

Following the successful detection and classification of the fault, the next step which is of considerable importance is the precise and fast fault location to reduce the downtime and repair costs and hence improve the availability and reliability of the transmission system. Therefore, some papers on fault location in AC and DC transmission lines have been researched and methods have been provided to determine the location of the fault.

Fault location methods in transmission lines are usually classified into three groups: impedance-based methods, traveling wave-based methods and learning-based methods [5,6]. The impedance-based methods are simple and low costs. In this methods, the synchronized voltage and current phasors obtained from phasor measurement units or intelligent electronic devices are employed to identify the fault line section and locate fault positions [7]. Other fault location methods, traveling wave-based methods and learning-based methods are widely used in both AC and DC transmission lines. Therefore, nowadays, the use of these methods has received much attention in the papers. The traveling wave-based methods have high accuracy and the results are not affected by the parameters, such as ground resistance or loading conditions [8]. The detection of traveling waves is done using methods such as correlation analysis, maximum likelihood estimation (MLE), adaptive

* Corresponding author.
E-mail address: mjoorabian@scu.ac.ir (M. Joorabian).

https://doi.org/10.1016/j.epsr.2023.109302
Received 27 December 2022; Received in revised form 28 February 2023; Accepted 6 March 2023
Available online 22 March 2023

filtering, mathematical morphology, empirical mode decomposition (EMD) and wavelet transform (WT).

Another classification of fault location methods in transmission lines is based on measurements they employ at receiving and/or sending ends of the transmission lines [9]. Therefore, these methods can be classified into two categories, single-ended and multi-ended methods. High reliability, no need for data communication and data synchronization, less complexity and lower costs are the attractions of fault location methods based on single-ended data [10]. Since the method used in this paper is based on traveling waves, in the following, papers with the method of fault location based on traveling waves have been reviewed.

The difference between the methods in the papers that have used traveling wave-based methods for fault location is the type of signal used (voltage or current) and sampling frequency. Most of the fault location schemes are based on voltage traveling wave propagation on the transmission line [11]. The use of discrete wavelet transform (DWT) in fault location in traveling wave based methods is first presented in [12]. Double-ended traveling wave-based fault location method using DWT in underground cables is presented in [13]. A traveling-wave based fault location method for two terminal HVAC transmission lines using unsynchronized current measurements from intelligent electronic devices (IEDs) recorded at both ends is presented in [14]. In this paper, first and second traveling wave arrival time and propagation velocity of the line are used for fault location. High sampling frequency is one of the weaknesses of the proposed method. In the single-ended method, the fault transients, which is reflected from the fault point and arrive at the relay terminals, produce a highly correlated signal for a delay time equal to twice the traveling time of the transients to the fault location. This time can be then used to find the distance from the relay to the fault location [11]. In [15,16], the single-ended traveling wave based method has been used to fault location in AC and DC transmission lines. In [16], a sampling frequency of 1 MHz was used and high impedance faults were not checked. [17] Has used the dominant natural frequency in the spectrum analysis of current traveling waves to locate faults in DC transmission lines. In [11], a comprehensive review on fault location in AC transmission lines based on current traveling waves using single-end and double-end data is presented. The sampling frequency used in this paper is 1.25 MHz, which is considered as a weakness for the proposed method.

In [18,19], the traveling wave based fault location principles for HVDC transmission lines are analyzed. This method is applicable in the single-ended or double-ended methods. The maximum fault location error is about 0.3% of the length of the transmission line. But the faulty half of transmission line identification method is not presented in this paper. In [8], a single-ended traveling wave based fault location method for segmented HVDC transmission line (an overhead line combined with an underground cable) is presented. In this paper, the normalized energies are used as the input to a binary Support Vector Machine (SVM) classifier for faulty section identification (underground cable or overhead line). In [20], by using the single-end voltage signal processing and mathematical morphology method, the reverse of the voltage traveling waves (RVTW) is calculated and used for fault location in HVDC transmission lines. The accuracy of fault location in this method is about 98% and the measurement error is about 1.44%. In [21], wavelet-based electromagnetic time reversal method using the current signals of both terminals of the transmission line is used to locate faults in VSC-HVDC transmission lines. In [7,22], a fault traveling wave-based location method for hybrid AC lines (underground cable and overhead transmission line) is proposed. In [7], the extreme-point symmetric mode decomposition (ESMD) method and Teager energy operator (TEO) are used to detect the arrival time of traveling waves.

In the papers presented above, fault location in HVAC or HVDC transmission lines has been investigated using the traveling wave method. In some papers, studies have been conducted on electromagnetic coupling between AC and DC lines in HPOTLs, and in a few published papers, fault detection in HPOTLs has been investigated [23–31]. But fault location in these lines, especially the AC/DC intersystem faults, is not presented in the papers. The purpose of this paper is to locate the fault in HPOTLs (AC and DC transmission lines on the same tower). In this paper, in addition to fault location in AC and DC transmission lines separately, fault location for AC/DC intersystem faults is also done with a similar method.

In all the simulations performed, electromagnetic coupling between AC and DC transmission lines is considered. Simulations are carried out by using PSCAD, and MATLAB (MATLAB Wavelet Toolbox) is used for data analysis and signal processing. The remainder of this paper is organized as follows: Section 2 explains the fault location principles and gives a brief introduction of DWT, traveling wave theory and Transmission line faulty half identification method. Section 3 describes the HPOTL modeling, and Section 4 discusses the simulation results. Sensitivity analysis of the proposed fault location method are presented in section 5. In section 6, the discussion and comparison of the results between different papers and the proposed method in the paper are presented and finally Section 7 concludes the paper.

2. Fault location principles

This section presents the principles of fault location in HPOTLs based on sending end voltage signals of transmission line. In the proposed method, the voltage signals of AC and DC transmission lines are sampled on sending end of transmission lines at the sampling rate of 100 kHz. After AC and DC voltage sampling, the modal components are extracted from the three-phase voltages of the AC line and the positive and negative pole voltages of the DC line. In this paper, the aerial mode of AC and line mode (1-mode) of DC voltage is used to calculate the location of AC, DC and AC/DC intersystem faults in transmission line. It should also be mentioned that in order to improve the estimation of the fault location in AC/DC intersystem faults that occur between AC and DC lines, the aerial mode of the voltage of both transmission lines (AC and DC) are used simultaneously and the fault location is calculated based on the averaging between them. The modal voltage signals are decomposed using the db4 wavelet for AC voltage (scale 1) and Haar wavelet (db1) for DC voltage signals (scale 2). The squared wavelet transform coefficients (WTC2) is used for proposed fault location method. The next step is to define whether the fault is in the first or second half of the transmission line. For this task polarities of first and second voltage traveling wave fronts can be used. Finally, by using the single ended traveling wave theory and using the Bewley-Lattice diagram, the location of the fault is estimated. In the following, Clarke and karrenbauer transformations for modal components extraction, DWT and traveling wave based fault location principle based on single ended data are presented.

In this paper, Clarke's transformation is used to decoupling the three-phase voltage in the HVAC system. The Clarke's transform is formulated as follows:

$$\begin{bmatrix} V_\alpha \\ V_\beta \\ V_0 \end{bmatrix} = \frac{2}{3} \begin{bmatrix} 1 & -\frac{1}{2} & -\frac{1}{2} \\ 0 & \frac{\sqrt{3}}{2} & -\frac{\sqrt{3}}{2} \\ \frac{1}{2} & \frac{1}{2} & \frac{1}{2} \end{bmatrix} \begin{bmatrix} V_a \\ V_b \\ V_c \end{bmatrix} \quad (1)$$

Where V_a, V_b and V_c represent the voltage values of the phase "A", "B" and "C" respectively; and V_α, V_β and V_0 represent the modal values. The first mode (1-mode) and second mode (2-mode) are known as the aerial mode and the 0-mode is referred to as the ground mode [12]. In this paper, 1-mode (V_α) is used to locate all AC faults, except for BC fault, 2-mode (V_β) is used.

The bipolar coupled line voltages can be decoupled to earth-mode (0-mode) and line-mode (1-mode) components according to the decoupling karrenbauer phase-mode matrix that given as follows [32]:

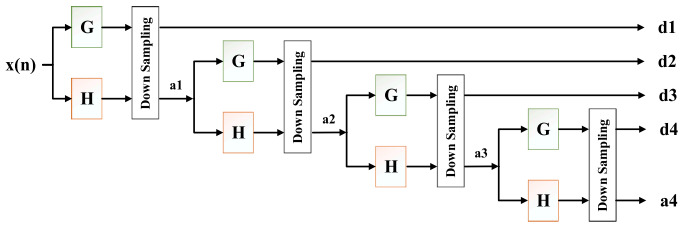

Fig. 1. Decomposition tree of discrete wavelet transform (DWT) (Four level of decomposition).

$$\begin{bmatrix} u_1 \\ u_0 \end{bmatrix} = \frac{1}{\sqrt{2}} \begin{bmatrix} 1 & -1 \\ 1 & 1 \end{bmatrix} \begin{bmatrix} u_+ \\ u_- \end{bmatrix} \tag{2}$$

Where u_1 is 1-mode voltage and u_0 is 0-mode voltage. Since u_m is in mode form, positive and negative voltage are decoupled and the effect of mutual inductances is eliminated. Considering that the 1-mode parameters are more stable than 0-mode parameters, the 1-mode parameters are used for fault location calculations in the HVDC line in this paper [32].

2.1. Discrete wavelet transform (DWT)

Wavelet analysis is a very powerful and practical signal processing method. This method is suitable for detecting sudden changes in a signal (transient phenomena). Therefore, it is widely used in fault location algorithms in electrical power systems. It should be noted that wavelet analysis does not use a time-frequency, but rather a time-scale region [33]. The analyzed signal is decomposed into different scales using a wavelet analysis function called the 'mother wavelet'. This wavelet is scaled and translated to match an input signal locally. The subsequent calculated wavelet coefficients represent the correlation between the (scaled) wavelet and the signal. Discrete Wavelet Transform (DWT) is introduced as a set of low-pass (called by H) and high-pass (called by G) filters. Such a structure, with four level of decomposition, has been shown in Fig. 1, where the original signal is decomposed into the approximation (a_j) and detail (d_j) coefficients. The discrete wavelet transform of a discrete signal x(k) is defined as:

$$DWT(m,k) = \frac{1}{\sqrt{a_0^m}} \sum_n x(n) \psi \left(\frac{k - nb_0 a_0^m}{a_0^m} \right) \tag{3}$$

Where, $\psi(0)$ is the mother wavelet.$a = a_0^m$ and $b = nb_0 a_0^m$ are represented as scaling and the translation parameter, respectively [34].

Some of the common wavelets used in the analysis of the transient studies of the power system, Signal processing and etc., are for example, Meyer, Daubechies (db), Morlet, Mexican Hat wavelet and etc. Modal voltage and current signals are processed using DWT to obtain the first level detail coefficients (D1). Haar wavelet, written as db1 is the simplest wavelet imaginable and is used in this paper as the mother wavelet in the analysis of HVDC waveforms. Also, db4 is used as the mother wavelet in the analysis of HVAC waveforms.

2.2. Traveling wave based fault location principle

In this paper, the single-ended traveling waves fault location method is used. As we know, fault location methods based on the single-ended transmission line signals have higher reliability and speed due to the lack of dependence on data from the remote end of the transmission line and also the elimination of the communication channel between the two ends of the transmission line. In single-ended fault location methods, all measurements are performed simultaneously on one end of the transmission line. In the fault location methods based on traveling waves, the location of fault is calculated based on the reflection time of the traveling waves from the fault point to the measuring terminal. In grounded faults, in addition to the waves received at the measuring terminal from the fault point, some waves are also reflected from the remote end of transmission line towards the measuring terminal. In the traveling wave's theory and using the Bewley-Lattice diagram, the waves received at the measuring terminal are similar to each other for faults with a symmetrical position relative to the middle of the transmission line. Therefore, the fault position in the first or second half of the transmission line should be determined using special algorithms [12]. Fig. 2 (a) and (b) shows waves propagation based on Bewley-Lattice diagrams for grounded and ungrounded faults, respectively. In the Bewley-lattice diagram, the following properties exist:

- In the path of traveling waves, time is increasing.
- The position of any wave at any time can be deduced directly from the diagram.
- The total voltage/current at any point, at any instant of time is the superposition of all the waves which have arrived at that point up

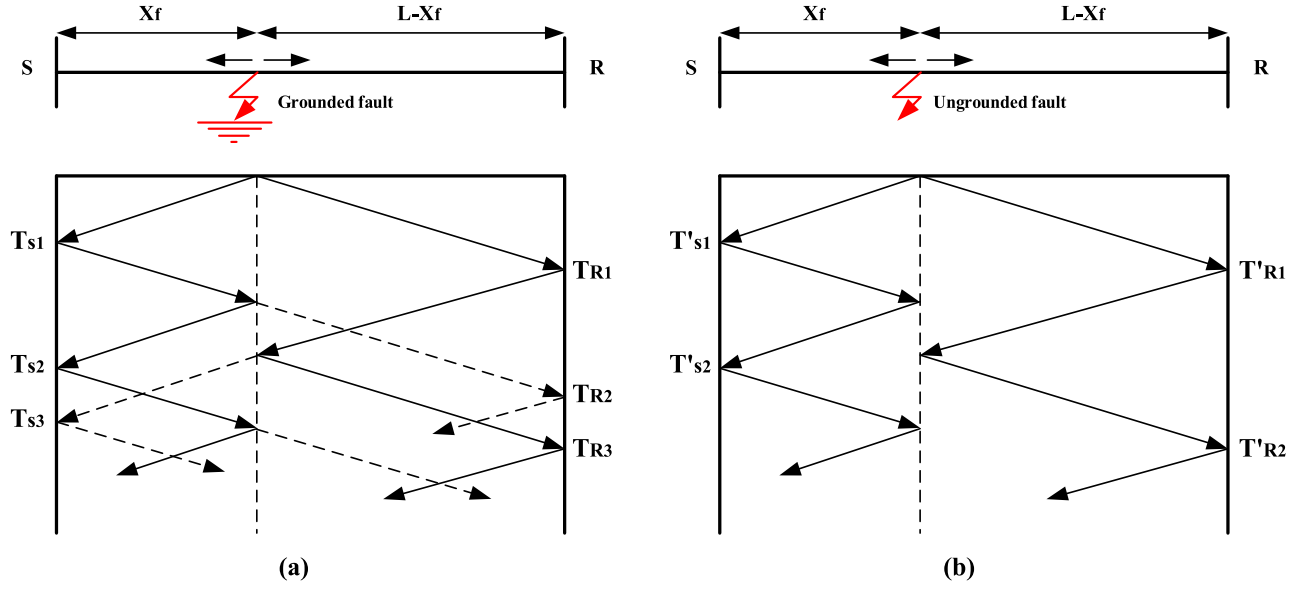

Fig. 2. Waves propagation based on Bewley-Lattice diagrams for (a) grounded and (b) ungrounded faults.

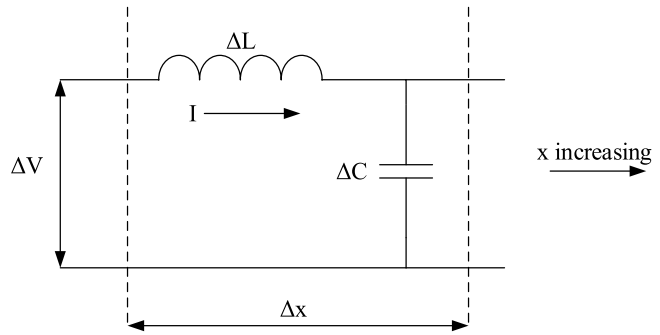

Fig. 3. Small element of a transmission line [36].

until that instant of time, displaced in position from each other by intervals equal to the difference in their time of arrival.

- The history of the wave is easily traced. It is possible to find where it came from and just what other waves went into its composition.

In this Fig. 2, X_f indicates the fault distance from the measuring terminal (terminal S) and L is the length of the transmission line.

According to the wave propagation model shown in Fig. 2, the location of the fault can be estimated based on the time of the waves received at terminal S. Following is the formulation of the problem for ungrounded and grounded faults:

2.2.1. Ungrounded faults

As mentioned in literatures, in ungrounded faults such as phase-to-phase fault in an AC transmission lines or pole-to-pole in a DC transmission lines, there is no significant reflection from remote end terminal during the fault transient, and the traveling waves between the fault point and transmission line terminals are moved (Fig. 2 (b)). Therefore, by measuring the time delay between two consecutive peaks in the discrete wavelet transform coefficients of the fault signal recorded in the desired scale and taking the product of the wave velocity and half of this time delay, the distance to the fault can easily be calculated for these kinds of faults [12,35]. In the following, the equation of calculating the fault location for ungrounded faults is presented.

$$X_f = \frac{\nu.(T'_{s2} - T'_{s1})}{2} \tag{4}$$

Where X_f is the distance of the fault from the terminal S, ν is the wave propagation velocity in the used mode of voltage and T'_{s1} and T'_{s2} are the peaks of the first and second waves on the DWT coefficients received to the terminal S, respectively.

2.2.2. Grounded faults

When a grounded fault occurs in the transmission line, unlike ungrounded faults, in addition to the traveling waves received at the terminal S from the fault point, waves are also reflected from the remote end terminal towards the terminal S Fig. 2 (a)). Also, depending on the location of the fault, the waves reflected from the remote end terminal (terminal R) may be received at the terminal S before or after the second wave reached the terminal S from the fault point. By using the Bewley-Lattice diagram, it can be concluded that if the fault occurs in the first half of the transmission line, the first and second waves received at terminal S are reflected from the fault point. But if the fault occurs in the second half of the transmission line, the first wave from fault point and the second wave have been reflected from the remote end terminal and reached the terminal S [12,35]. According to the previous explanations and assuming that the fault detection and classification algorithm has detected the type of fault as grounded fault, the faulty half of the transmission line should be identified. After faulty half determination, by using Eq. (5) and ((6), the fault location can be estimated for the faults of the first half and the second half of the transmission line, respectively.

$$X_f = \frac{\nu.(T_{s2} - T_{s1})}{2} \tag{5}$$

$$X_f = L - \frac{\nu.(T_{s2} - T_{s1})}{2} \tag{6}$$

Where X_f is the distance of the fault from the terminal S, ν is the wave propagation velocity in the used mode of voltage and T_{s1} and T_{s2} are the peaks of the first and second waves on the DWT coefficients received to the terminal S, respectively.

2.3. Faulty half of transmission line identification

The faulty half identification method presented in [35,36] is used in this paper. According to the of traveling waves theory, when a short circuit (SC) fault occurs in the transmission line, the voltage traveling waves with the same sign move from the fault point to both end of the transmission line (For example, in Fig. 4, the voltage traveling waves are shown with a positive sign). When the traveling wave reaches the end of the transmission line, some energy passes through the termination circuit and the rest is reflected towards the fault point. The reflection coefficient and its sign at the station termination depend on the termination circuit, but the sign of the reflection coefficient of the voltage is opposite to the current. If the station termination is capacitive, the voltage reflection coefficient is negative and if the station termination is inductive, the voltage reflection coefficient is positive. But in both cases, the transmission coefficient is positive. The return traveling wave from the end of the transmission line hits the fault point (SC) and some of its energy passes through the fault and the rest of it is reflected towards the end of the transmission line and this movement continues until the energy of the traveling wave becomes zero. Since the faults investigated in this paper are SC fault types, the reflection coefficient is positive. It should be noted that the transmission coefficient of traveling waves is always positive at the fault point. In the following, the traveling wave's equations and the reflection and transmission coefficients in transmission lines are presented.

In the studies presented in this section and to show the traveling waves equations, the line is assumed loss-less. Fig. 3 shows a small element of a transmission line with an inductance L (H/m), a capacitance C (F/m) and an elementary length Δx will have inductance LΔx and capacitance CΔx and as shown [36].

Voltage across the element and the current to charge the elementary capacitance CΔx are defined as follows:

$$\frac{\partial V}{\partial x} = -L\frac{\partial I}{\partial t} \tag{7}$$

$$\frac{\partial I}{\partial x} = -C\frac{\partial V}{\partial t} \tag{8}$$

By differentiating Eq. 7 with respect to 'x' and Eq. 8 with respect to 't' and integrating them together, equations for the voltage and current of the transmission line can be obtained separately:

$$\frac{\partial^2 V}{\partial x^2} = -L\frac{\partial^2 I}{\partial x \partial t}, \quad \frac{\partial^2 I}{\partial x \partial t} = -C\frac{\partial^2 V}{\partial^2 t}$$

$$\frac{\partial^2 V}{\partial x^2} = LC\frac{\partial^2 V}{\partial^2 t} \tag{9}$$

$$\frac{\partial^2 I}{\partial x^2} = LC\frac{\partial^2 I}{\partial^2 t} \tag{10}$$

By solving Eq. 9, it can be seen that the current equation will be in the form of Eq. 11:

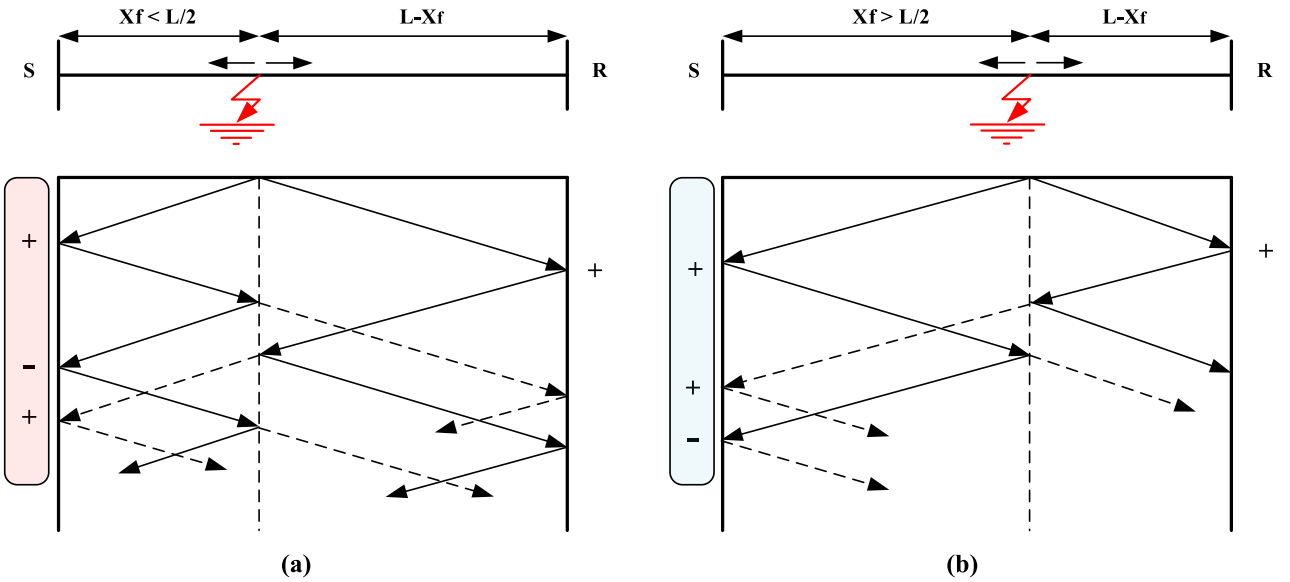

Fig. 4. Bewley-Lattice diagram for voltage traveling waves for (a) first and (b) second half transmission line faults.

$$I = f\left[x \pm \frac{t}{\sqrt{LC}}\right] \tag{11}$$

As we know, $(L/C)^{-1/2}$ is a velocity. Therefore, using Eq. 11, the current equation is obtained as Eq. 12. Also, Eqs. 7 and 12 have been used to obtain the Eq. 13 for voltage:

$$\begin{aligned} &I(x,t) = f_1(x-\nu t) + f_2(x+\nu t) \\ &\frac{\partial V}{\partial x} = -L\frac{\partial I}{\partial t} = L\nu[f'_1(x-\nu t) - f'_2(x+\nu t)] \end{aligned} \tag{12}$$

$$V(x,t) = L\nu[f_1(x-\nu t) - f_2(x+\nu t)] = Z_0 f_1(x-\nu t) - Z_0 f_2(x+\nu t) \tag{13}$$

In the voltage and current equations presented above, $f_1(x\text{-}\nu t)$ and $f_2(x+\nu t)$ represent traveling waves moving in the direction of plus x and moving in the direction of minus x with a velocity ν, respectively. In other words, traveling waves in the forward and backward directions. The difference between voltage and current is characteristic impedance (Z_0). Since the signs of the terms in the voltage and current equations show the direction of the traveling waves in the transmission line, the sign of the second term in the voltage equation is very important. We also note that current and voltage waves traveling in the positive direction of x have the same sign, whereas those traveling the negative direction have opposite sign [36]. In the following, the reflection and transmission coefficients of traveling waves in transmission lines have been investigated.

When the wave reaches a discontinuity in the transmission line so that the characteristic impedance of the transmission line changes, some of the wave is reflected back and the rest of the wave penetrates beyond the discontinuity. Consider the junction between lines of characteristic impedance Z_A and Z_B and it is assumed that $Z_A > Z_B$ [36]. Suppose the voltage surge reaches the discontinuity with a step function and with amplitude V_1. At this moment, the amplitude of the corresponding current wave is equal to:

$$I_1 = \frac{V_1}{Z_A} \tag{14}$$

If the reflected and transmitted traveling wave's voltage is equal to V_2 and V_3, respectively, the reflected and transmitted traveling wave's current are equal to:

$$I_2 = \frac{-V_2}{Z_A} \tag{15}$$

$$I_3 = \frac{V_3}{Z_B} \tag{16}$$

According to the explanations given earlier, since the traveling waves of voltage and current in the direction of minus x have opposite signs, the negative sign is included in Eq. 15. If voltage and current are to be continuous at the junction, it follows that:

$$V_1 + V_2 = V_3 \quad , \quad I_1 + I_2 = I_3 \tag{17}$$

Using Eqs. (14–17) and combining them, the reflection and transmission coefficients for the voltage traveling wave can be obtained as follow:

$$V_2 = \left(\frac{Z_B - Z_A}{Z_B + Z_A}\right) V_1 \rightarrow V_2 = aV_1, \; -1 \le a \le 1 \tag{18}$$

$$V_3 = \left(\frac{2Z_B}{Z_B + Z_A}\right) V_1 \rightarrow V_3 = bV_1, \; 0 \le b \le 2 \tag{19}$$

$$a = \frac{Z_B - Z_A}{Z_B + Z_A}, \quad b = \frac{2Z_B}{Z_B + Z_A}, \quad Z_A = \sqrt{\frac{L}{C}} \tag{20}$$

In the above equations, 'a' is the reflection coefficient and 'b' is the transmission coefficient. Examples of discontinuity points are short circuit points and transmission line terminals (both end of transmission line), for which reflection and transmission coefficients should be calculated. In short circuit faults points, the fault impedance (Z_B) in normal faults is lower than the characteristic impedance (Z_A) of the line, and according to Eqs. 18 and 19, it can be seen that for the voltage traveling wave, the reflection coefficient will be a negative value and the transmission coefficient will be a positive value. Therefore, when the voltage traveling wave meets the short circuit point, the reflected voltage wave will have the opposite sign to the original wave. For the open circuit (OC) faults, if we assume the impedance of the open circuit to be infinite ($Z_B \rightarrow \infty$), the sign of the reflection coefficient and transmission coefficient for the voltage traveling wave will be the same as the initial wave. But, the calculation of the reflection and transmission coefficients at both ends of the transmission line depends on the termination circuit, and different values are obtained depending on whether the circuit is capacitive or inductive. Since the termination circuit of the presented transmission line model in this paper is inductive, in this section the reflection and transmission coefficients for inductive mode are presented.

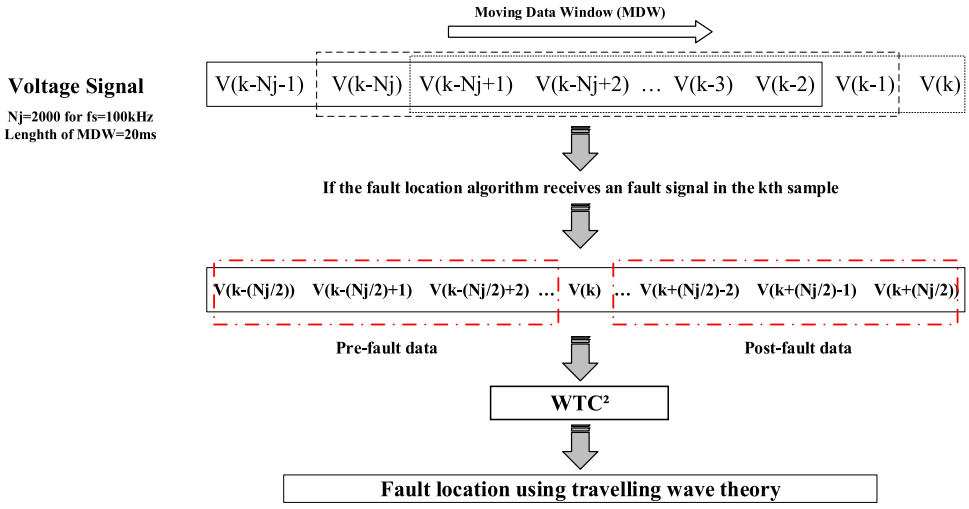

Fig. 5. Method of voltage signals sampling (create a data window for fault location).

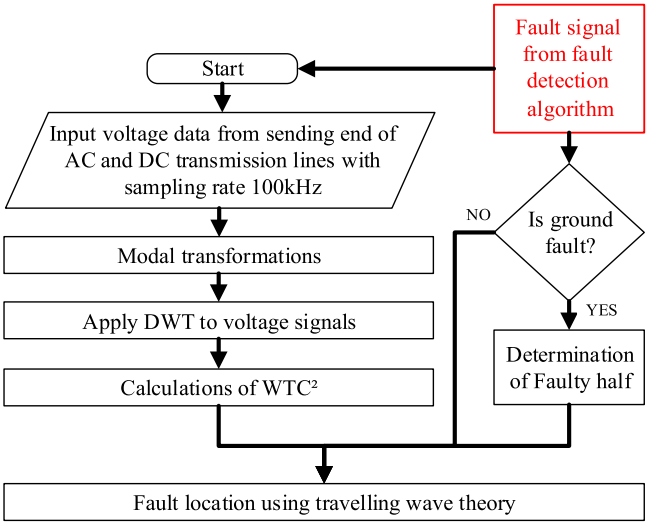

Fig. 6. Flowchart of the proposed fault location algorithm.

Suppose the voltage wave travels on the transmission line with characteristic impedance Z_A and impinges the terminal equipment with Z_B impedance. According to Eq. 21, Z_A is independent of 'S' (frequency), but the value of Z_B (inductive impedance) in depends on 'S'.

$$Z_A = \sqrt{\frac{Ls}{Cs}} = \sqrt{\frac{L}{C}}, \quad Z_B = L_1 s \tag{21}$$

Using Eqs. 18, 19 and 21, the reflection and transmission coefficients can be calculated in terms of 'S' as follows, assuming that the initial voltage traveling wave is a step function with amplitude V_1:

$$u_2(s) = a u_1(s) = \frac{V_1}{s}\left[\frac{L_1 s - Z_A}{L_1 s + Z_A}\right] = \frac{V_1}{s}\left[\frac{s - (Z_A/L_1)}{s + (Z_A/L_1)}\right] \tag{22}$$

$$u_3(s) = b u_1(s) = \frac{V_1}{s}\left[\frac{2L_1 s}{L_1 s + Z_A}\right] = \frac{V_1}{s}\left[\frac{2s}{s + (Z_A/L_1)}\right] \tag{23}$$

Table 1
HPOTL system specifications.

HVAC SYSTEM		HVDC SYSTEM	
Power	400 MW	Power	1000 MW
Voltage	400 kV	Voltage	± 500 kV
Frequency	50 Hz	Current (per pole)	1000 A
AC Trans. MVA	750 MVA	V_{ac}-Rec (L-L)/ V_{ac}-Inv (L-L)	345/230 kV
AC Filter	11th, 13th, HP and fixed shunt capacitor	DC Filter	12th, HP
TRANSMISSION LINE CONDUCTORS			
Total Bundled	3	SAG (all conductors)	10 m
Sub-Conductors Spacing	0.4 m	Ground Resistivity	100 Ω.m
DC Resistance	0.0394 Ω/km	Number of Ground Wire	2

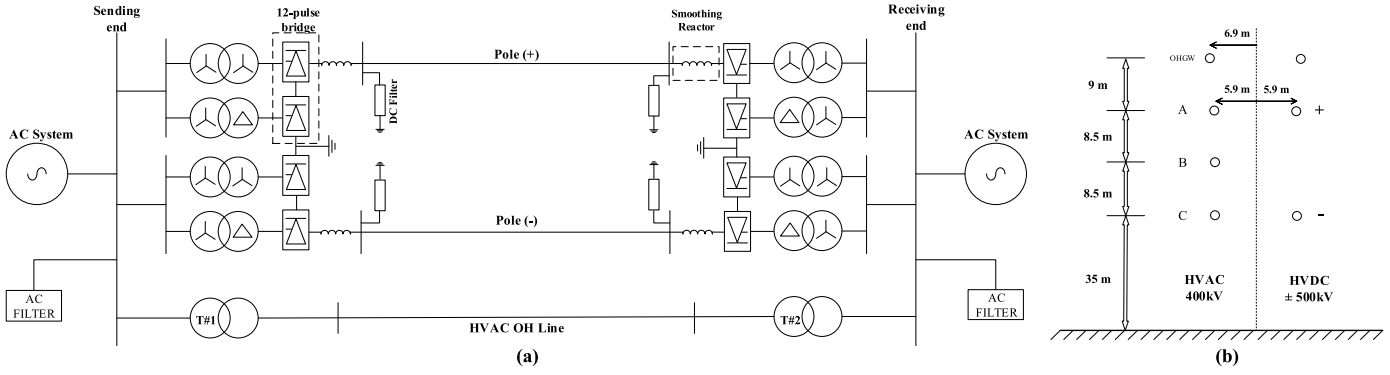

Fig. 7. (a) HPOTL model and (b) HPOTL tower configuration.

Table 2
Types of faults in the HPOTLs and the components used for fault location.

Faults classification	Fault types		Component used for fault location
DC faults	Pole to ground	SPGF	Second detail component of line mode (1-mode) of DC voltage
	Pole to pole	PPF	(V_{dc1}-Scale 2-Haar wavelet)
	Pole to pole to ground	PPGF	
AC faults	Phase to ground	SLGF	First detail component of areal mode (1-mode) of AC voltage (V_{ac1}-Scale 1-db4 wavelet)
	Phase to phase	LLF	Except for BC fault (phase B to C)
	Phase to phase to ground	LLGF	First detail component of areal mode (2-mode) of AC voltage (V_{ac2}-Scale 1-db4 wavelet)
	Three phase	LLLF	
AC/DC intersystem faults	Phase to pole	LPF	First detail component of areal mode (1-mode) of AC voltage
	Phase to pole to ground	LPGF	(V_{ac1}-Scale 1-db4 wavelet)
	Phase to two pole	LPPF	Except for BCP and BCN fault (phase B to C to pole)
	Phase to two pole to ground	LPPGF	First detail component of areal mode (2-mode) of AC voltage
	Phase to phase to pole	LLPF	(V_{ac2}-Scale 1-db4 wavelet)
	Phase to phase to pole to ground	LLPGF	**and**
	Two phase to two pole	LLPPF	Second detail component of line mode (1-mode) of DC voltage
	Two phase to two pole to ground	LLPPGF	(V_{dc1}-Scale 2-Haar wavelet)
	Three phase to pole	LLLPF	
	Three phase to pole to ground	LLLPGF	
	Three phase to two pole	LLLPPF	
	Three phase to two pole to ground	LLLPPGF	

$$(L_1 / Z_A) = (1/\alpha) \rightarrow u_2(s) = V_1\left[\frac{1}{(s+\alpha)} - \frac{\alpha}{s(s+\alpha)}\right] \quad (24)$$

$$u_3(s) = V_1\left[\frac{2}{(s+\alpha)}\right] \quad (25)$$

The reflection and transmission coefficients in terms of 't' are calculated as follows:

$$V_2(t) = -V_1(1-2e^{-\alpha t}) \quad (26)$$

$$V_3(t) = 2V_1 e^{-\alpha t} \quad (27)$$

Using Eqs. 26 and 27, it can be concluded that when the wave arrives at its terminals, momentarily it appears like an open circuit and so that ultimately it appears as a short circuit [36]. Therefore, the voltage wave is reflected and transmitted at the moment of impact with the same sign as the initial wave, and the sign of the reflection and transmission coefficients becomes positive. According to the explanations provided in this section, Bewley-Lattice diagram for voltage traveling waves for first and second half transmission line faults is presented in Fig. 4.

According to the sign of voltage traveling waves received at the terminal 'S', it can be found that the fault occurred in the first or in the second half of the transmission line. As can be seen in Fig. 4, when the fault occurs in the first half of the transmission line, the first and second waves received at terminal 'S' have opposite signs (+/- or -/+), and when the fault occurs in the second half of the transmission line, the first and second waves received at terminal 'S' have the same (+/+ or -/-). This issue can be understood by comparing polarity of the first and second observed voltage traveling waves. In this paper, the 1-mode of AC voltage is used to faulty half of transmission line identification in AC and AC/DC intersystem faults, and the 1-mode of DC voltage is used to faulty half of transmission line identification in DC faults.

2.4. Proposed fault location method

The presented method for fault location is that the AC and DC voltage signals from sending end of transmission lines are sampled with a sampling rate of 100 kHz and stored in a moving data window with a length of 20 ms. As soon as the fault occurs and the fault is detected by

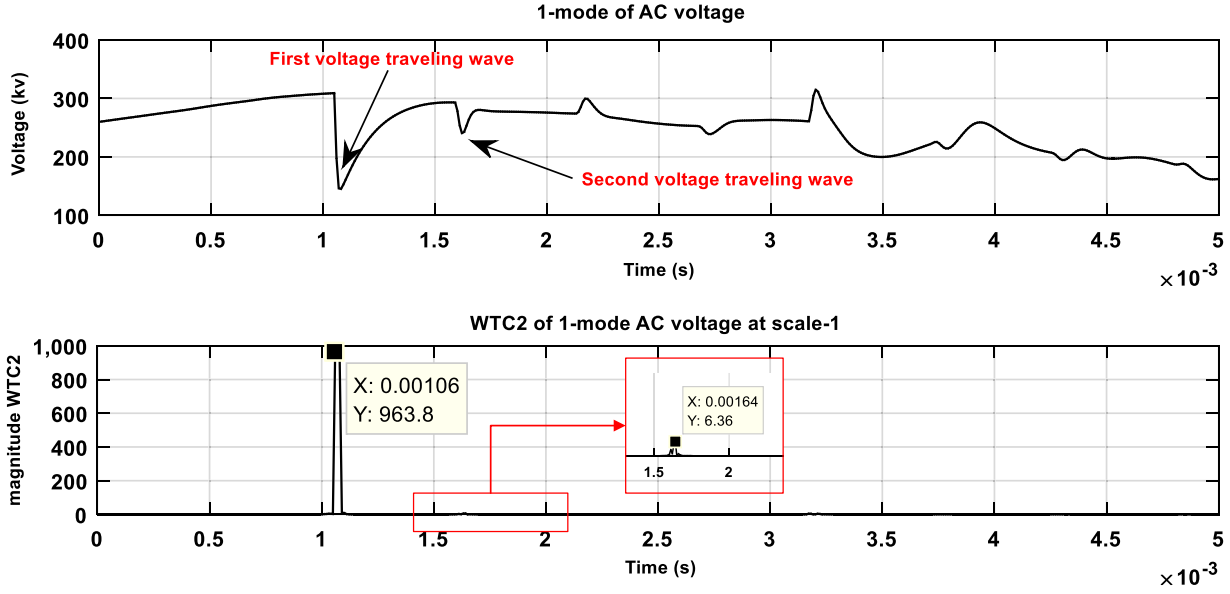

Fig. 8. (Up) 1-mode of AC voltage and (down) AC voltage WTC^2 at scale-1 under SLGF (A to ground fault) at x=318 km.

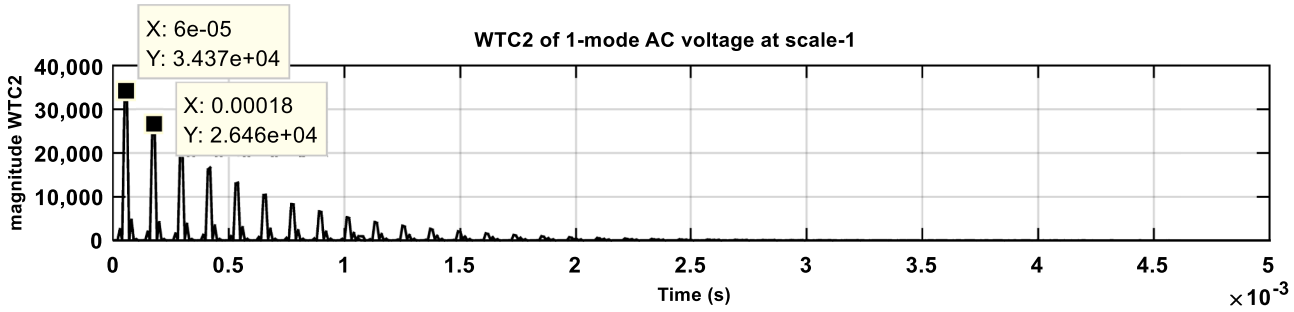

Fig. 9. AC voltage WTC^2 at scale-1 under LLF (A to B fault) at x=18 km.

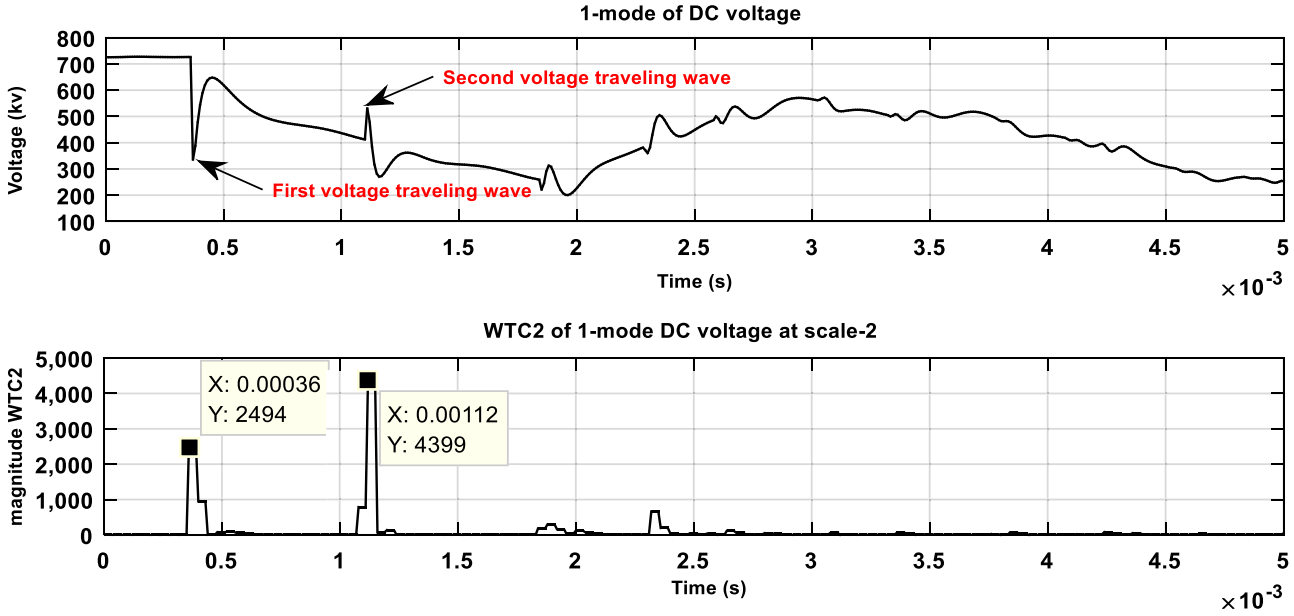

Fig. 10. (Up) 1-mode of DC voltage and (down) DC voltage WTC^2 at scale-2 under SPGF (positive pole to ground fault) at x=111 km.

the protection algorithms, the fault detection signal is sent to fault location algorithm and the sampling of AC and DC voltage will continue for 10 ms and is stored in the data window. There are now 10 ms of pre-fault voltage samples and 10 ms of post-fault voltage samples in the data window, which is enough to locate the fault. By using signal processing based on DWT on the data window, the location of the fault can be found. In the following, the steps of the proposed method for fault location in HPOTL lines are presented.

The process of the proposed fault location method for HPOTLs goes through the following steps:

- Sampling of AC and DC voltage signals from sending end of transmission lines with a sampling rate of 100 kHz and stored in a moving data window with a fixed length of 20 ms.
- When the fault detection signal is received by the fault location algorithm, the sampling of AC and DC voltage will continue for 10 ms and is stored in the data window.
- Perform modal transformations (Clarke and Karrenbauer transformations) on AC and DC voltage signals on data window.
- Apply DWT to voltage signal.
- Calculation of squared wavelet transform coefficients (WTC^2) for voltage signals.
- Determination of faulty half of transmission line for grounded faults by comparing polarity of the first and second observed voltage traveling waves.
- Using traveling wave theory and Bewley-Lattice diagram to locate the fault.

As mentioned above, the method of voltage signals sampling (create a data window for fault location) and the flowchart of the proposed fault location algorithm are shown in Figs. 5 and 6, respectively.

3. Hybrid parallel HVAC/HVDC overhead transmission line (HPOTL) modeling

In this section, the used model of hybrid parallel HVAC/HVDC overhead transmission line is presented to study and simulate fault location in AC and DC lines. Fig. 7 shows the model of a HPOTL on the same tower and tower configuration simulated in this paper. Electromagnetic coupling between AC and DC lines is considered as one of the main challenges in HPOTLs. Therefore, voltage and current components are induced in HVAC and HVDC transmission line under different operating conditions, normal and transient conditions (fundamental frequency components in the DC line and the DC component in the AC line). Voltage and current equations of electromagnetic coupling between lines in parallel transmission lines are presented in the appendix. It should be noted that, transmission lines transposition is considered in this model and all voltage and current waveforms shown are from the sending end of transmission line. Simulated model in PSCAD software includes a 400 kV, 400 MW, 50 Hz ac single circuit with a ±500 kV, 1000 MW dc circuit connected into the same receiving and sending end ac systems. DC section is a bipolar CIGRE 12 pulse HVDC model and the DC controls are based on the CIGRE benchmark model [37]. The total length of HPOTL is 400 km. As shown in Fig. 7, AC filters in bus A and bus B (11th, 13th and High Pass filter) are added to absorb the harmonics generated by the converter as well as together with a fixed shunt

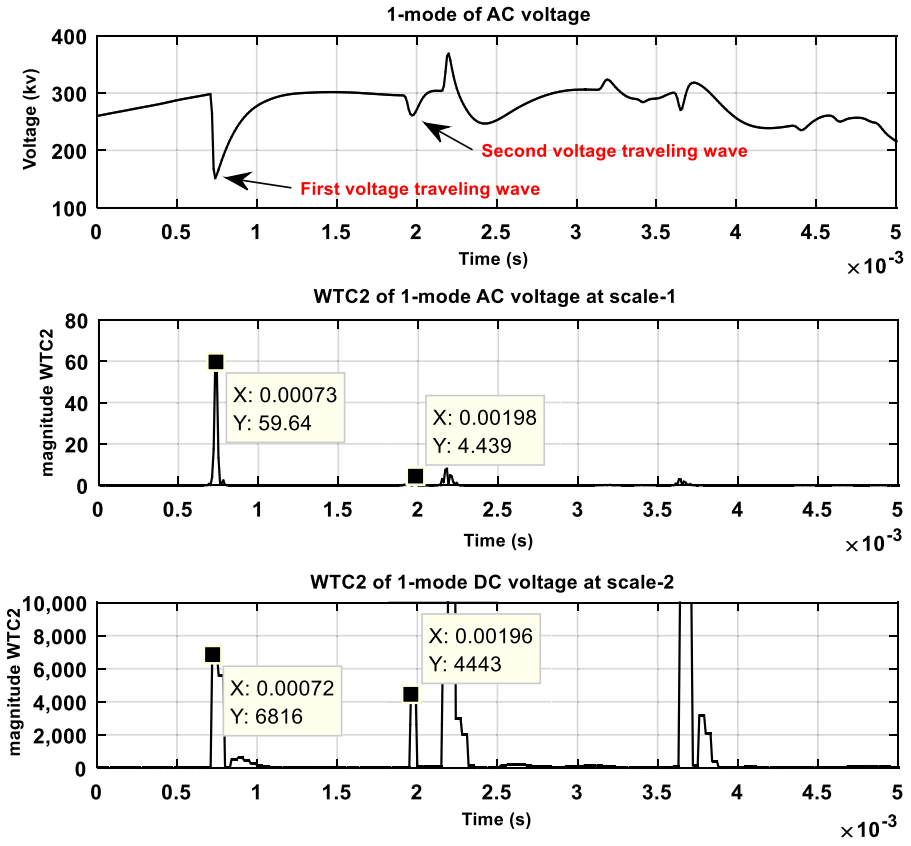

Fig. 11. (Up) 1-mode of AC voltage, (middle) AC voltage WTC^2 at scale-1 and (down) DC voltage WTC^2 at scale-2 under LPPGF (phase A to PN to ground fault) at x=218 km.

Table 3
Some examples for AC fault location in AC transmission line in HPOTLs.

Fault type		Fault	Xact (km)	1st sample	2nd sample	ΔS sample	Polarity of the 1st and 2nd wave	Faulty half	Xcal (km)	ABS (error %)
AC Faults	**SLGF**	**AG**	24	9	25	16	Opposite	First	23.60	**0.10**
			98	35	101	66	Opposite	First	97.35	**0.16**
			215	73	197	124	Same	Second	217.10	**0.52**
			318	106	164	58	Same	Second	314.45	**0.89**
	LLF	**AB**	18	6	18	12	-	-	17.70	**0.07**
			131	45	132	87	-	-	128.33	**0.67**
			218	74	221	147	-	-	216.83	**0.29**
			341	115	345	230	-	-	339.25	**0.44**
		BC	41	15	42	27	-	-	39.83	**0.29**
			117	38	117	79	-	-	116.53	**0.12**
			205	68	206	138	-	-	203.55	**0.36**
			362	121	367	246	-	-	362.85	**0.21**
	LLGF	**ACG**	19	6	19	13	Opposite	First	19.18	**0.04**
			122	43	125	82	Opposite	First	120.95	**0.26**
			221	75	195	120	Same	Second	223.00	**0.50**
			346	117	153	36	Same	Second	346.90	**0.22**
	LLLF	**ABC**	31	10	31	21	-	-	30.98	**0.01**
			109	36	111	75	-	-	110.63	**0.41**
			231	77	232	155	-	-	228.63	**0.59**
			333	111	335	224	-	-	330.40	**0.65**

capacitor to supply reactive power to the converter. DC smoothing reactors installed in series with the poles of the HVDC transmission line are 0.5968 H. Also a high-pass DC filter tuned to the 12th harmonic is placed on the DC side. HPOTL system specifications are given in Table 1.

4. Simulations results

Simulation results for fault location in HPOTLs according to the model presented in Section 3 are presented in this section. The length of the HPOTL is 400 km, and both systems (HVAC and HVDC transmission lines) are parallel to each other in the entire line and are on the same tower (Fig. 7). The frequency dependent line model is used for transient studies. The simulation time step in 10 μs and the sampling rate is 100 kHz. Simulations are carried out by using PSCAD software and MATLAB software (MATLAB Wavelet Toolbox) is used for data analysis and signal processing. The voltage traveling wave velocity for areal mode is assumed to be 2.95×10^5 km/s. As mentioned before, in this paper, it is assumed that the occurrence of the fault (AC, DC and AC/DC intersystem fault) and its classification (detection of the faulty pole and/or faulty phase) has been detected by a protection algorithm. Since the presented

Table 4
Some examples for DC fault location in DC transmission line in HPOTLs.

Fault type		Fault	Xact (km)	1st sample	2nd sample	ΔS sample	Polarity of the 1st and 2nd wave	Faulty half	Xcal (km)	ABS (error %)
DC Faults	**SPGF**	**PG**	21	5	21	16	Opposite	First	23.60	**0.65**
			111	37	113	76	Opposite	First	112.10	**0.28**
			234	77	189	112	Same	Second	234.80	**0.20**
			371	125	144	19	Same	Second	371.98	**0.24**
		NG	32	9	33	24	Opposite	First	35.40	**0.85**
			127	41	129	88	Opposite	First	129.80	**0.70**
			254	85	185	100	Same	Second	252.50	**0.38**
			346	117	153	36	Same	Second	346.90	**0.22**
	PPF	**PN**	18	5	17	12	-	-	17.70	**0.07**
			105	33	105	72	-	-	106.20	**0.30**
			243	81	245	164	-	-	241.90	**0.27**
			351	117	353	236	-	-	348.10	**0.72**
	PPGF	**PNG**	15	5	17	12	Opposite	First	17.70	**0.68**
			118	41	121	80	Opposite	First	118.00	**0.00**
			210	69	200	131	Same	Second	206.78	**0.81**
			348	117	153	36	Same	Second	346.90	**0.28**

fault location method is based on the singe end data of the transmission line, only the voltage data of the sending end of the transmission line has been used to fault location and faulty half determination.

Different type of balanced and unbalanced faults such as AC, DC and AC/DC intersystem faults at different locations along the line are simulated. The types of faults in the HPOTLs and the components used for fault location are presented in Table 2. As shown in this Table, in HPOTLs there are 5 types of AC faults, 3 types of DC faults and 12 types of AC/DC intersystem faults. All of AC, DC and intersystem faults have been simulated for fault location method validation. But in this section, fault location is presented only for 4 different cases (two case for AC faults and one case for each of DC and AC/DC intersystem faults) using the proposed method based on traveling waves. Also, the effectiveness of the proposed fault location method is evaluated using the error which is calculated as a percentage of the total system length as:

$$Error\,(\%) = \left|\frac{Actual\ fault\ location - calculated\ fault\ location}{Total\ length\ of\ transmission\ line}\right| \times 100 \quad (28)$$

4.1. Case 1: AC fault: phase A to ground fault (SLGF)

The first case is the phase A to ground fault (SLGF) in the AC line at 318 km from the sending end of the transmission line. Since the fault under study is a grounded fault, the faulty half of the transmission line should be identified. The waveforms of 1-mode AC voltage from the sending end of the transmission line and the WTC[2] for AC voltage at scale-1 for SLGF are shown in Fig. 8.

As can be seen in Fig. 8 (up), the polarity of the first and second voltage traveling waves are the same (both are negative). According to what was presented at the end of section 2.3, it can be concluded that the fault occurred in the second half of the transmission line. In Fig. 8 (down), the first and second DC voltage traveling waves received at sending end of transmission line and their arrival time are specified. Therefore, by using the time difference of two received waves and using Eq. 6, the location of the fault can be obtained as follows:

$$X_f = L - \frac{\nu.(T_{s2} - T_{s1})}{2} = 400 - \frac{2.95 \times 10^5 \times (0.00164 - 0.00106)}{2} = 314.45\ km$$

Using Eq. 28, it is possible to estimate the error of fault location at proposed method. The fault location error in this case is calculated as follows:

$$Error\,(\%) = \left|\frac{318 - 314.45}{400}\right| \times 100 = 0.8875\%$$

4.2. Case 2: AC fault: phase to phase (A to B) fault (LLF)

The second case is the phase to phase (A to B) fault (LLF) in the AC line at 18. Since the fault under study is an ungrounded fault, it is not required to identify the faulty half of the transmission line and fault location is calculated using traveling wave theory for ungrounded faults (Eq. 4). The waveforms of the WTC[2] for AC voltage at scale-1 for LLF are shown in Fig. 9.

$$X_f = \frac{\nu.(T'_{s2} - T'_{s1})}{2} = \frac{2.95 \times 10^5 \times (0.00018 - 0.00006)}{2} = 17.7\ km$$

Using Eq. 28, the fault location error for this case is calculated 0.07%.

4.3. Case 3: DC fault: positive pole to ground fault (SPGF)

The third case is the positive pole to the ground fault (SPGF) in the DC line at 111 km. The waveforms related to 1-mode DC voltage from the sending end of the transmission line and the WTC[2] for DC voltage at scale-2 are shown in Fig. 10.

As can be seen in Fig. 10 (up), the polarity of the first and second voltage traveling waves are opposite. According to what was presented at the end of section 2.3, it can be concluded that the fault occurred in the first half of the transmission line. In Fig. 10 (down), the first and second DC voltage traveling waves received at sending end of transmission line and their arrival time are specified. Therefore, by using the time difference of two received waves and using Eq. 5, the location of the fault can be obtained as follows:

$$X_f = \frac{\nu.(T_{s2} - T_{s1})}{2} = \frac{2.95 \times 10^5 \times (0.00112 - 0.00036)}{2} = 112.1\ km$$

Using Eq. 28, the fault location error for this case is calculated 0.275%.

4.4. Case 4: AC/DC intersystem fault- phase to two pole (B to PN) to ground fault (LPPGF)

The fourth case is the phase to two pole (B to PN) to ground fault (LPPGF) between the AC and DC line at 218 km from the sending end of the transmission line. Similar to case 1 and 3, in this case also the faulty half of the transmission line should be identified. As shown in Table 2, the number of intersystem faults is large, and in this section, the LPPGF is examined as an example of this type of fault. Since the AC/CD intersystem faults occurs between the phases of the AC system and the poles of the DC system and involves both systems in fault, in this paper in order to locate these faults, the AC and DC voltage components are used. AC voltage component is used to faulty half of transmission line identification in intersystem faults type. But the proposed fault location

Table 5
Some examples for AC/DC intersystem fault location in HPOTLs.

Fault type		Fault	Xact (km)	1st sample	2nd sample	ΔS sample	Polarity of the 1st and 2nd wave	Faulty half	Xcal (km)	Error %	Final Xcal (km)	ABS (total error %)
AC/DC intersystem Faults	**LPF**	**AP**	35	13	37	24	-	-	35.40	0.10	**36.87**	**0.47**
				13	39	26	-	-	38.35	0.84		
			350	117	353	236	-	-	348.10	-0.47	**349.57**	**0.11**
				117	355	238	-	-	351.05	0.26		
	LPGF	**BPG**	190	65	193	128	Opposite	First	188.80	-0.30	**189.53**	**0.12**
				62	191	129	Opposite	First	190.28	0.07		
			371	125	144	19	Same	Second	371.98	0.24	**371.23**	**0.06**
				125	145	20	Same	Second	370.50	-0.13		
	LPPF	**APN**	122	41	125	84	-	-	123.90	0.48	**122.42**	**0.11**
				43	125	82	-	-	120.95	-0.26		
			221	73	225	152	-	-	224.20	0.80	**221.25**	**0.06**
				75	223	148	-	-	218.30	-0.67		
	LPPGF	**BPNG**	45	13	45	32	Opposite	First	47.20	0.55	**45.72**	**0.18**
				15	45	30	Opposite	First	44.25	-0.19		
			318	105	161	56	Same	Second	317.40	-0.15	**317.4**	**0.15**
				106	162	56	Same	Second	317.40	-0.15		
	LLPF	**BCP**	130	45	133	88	-	-	129.80	-0.05	**130.53**	**0.13**
				42	131	89	-	-	131.28	0.32		
			230	77	233	156	-	-	230.10	0.03	**228.62**	**0.34**
				77	231	154	-	-	227.15	-0.71		
		ABP	62	25	69	44	-	-	64.90	0.73	**63.42**	**0.36**
				23	65	42	-	-	61.95	-0.01		
			341	113	345	232	-	-	342.20	0.30	**339.98**	**0.25**
				115	344	229	-	-	337.78	-0.81		
	LLPGF	**ABNG**	29	9	29	20	Opposite	First	29.50	0.13	**28.76**	**0.06**
				11	30	19	Opposite	First	28.03	-0.24		
			381	138	153	15	Same	Second	377.88	-0.78	**378.61**	**0.60**
				126	140	14	Same	Second	379.35	-0.41		
	LLPPF	**ACPN**	110	41	117	76	-	-	112.10	0.53	**110.62**	**0.16**
				39	113	74	-	-	109.15	-0.21		
			242	81	245	164	-	-	241.90	-0.02	**241.9**	**0.02**
				82	246	164	-	-	241.90	-0.02		
	LLPPGF	**ABPNG**	111	37	113	76	Opposite	First	112.10	0.28	**110.62**	**0.09**
				37	111	74	Opposite	First	109.15	-0.46		
			345	113	149	36	Same	Second	346.90	0.47	**345.42**	**0.11**
				115	153	38	Same	Second	343.95	-0.26		
	LLLPF	**ABCP**	25	9	25	16	-	-	23.60	-0.35	**23.6**	**0.35**
				8	24	16	-	-	23.60	-0.35		
			228	77	233	156	-	-	230.10	0.53	**227.88**	**0.03**
				77	230	153	-	-	225.68	-0.58		
	LLLPGF	**ABCNG**	150	49	153	104	Opposite	First	153.40	0.85	**150.45**	**0.11**
				51	151	100	Opposite	First	147.50	-0.63		
			355	117	149	32	Same	Second	352.80	-0.55	**353.53**	**0.37**
				118	149	31	Same	Second	354.28	-0.18		
	LLLPPF	**ABCPN**	61	21	61	40	-	-	59.00	-0.50	**60.47**	**0.13**
				20	62	42	-	-	61.95	0.24		
			320	105	321	216	-	-	318.60	-0.35	**320.07**	**0.02**
				107	325	218	-	-	321.55	0.39		
	LLLPPGF	**ABCPNG**	177	57	177	120	Opposite	First	177.00	0.00	**176.26**	**0.18**
				59	178	119	Opposite	First	175.53	-0.37		
			210	69	197	128	Same	Second	211.20	0.30	**211.2**	**0.30**
				71	199	128	Same	Second	211.20	0.30		

method in this paper suggests a new method to increase the accuracy of calculating the fault location for AC/DC intersystem faults. In this paper, for intersystem fault location, the average location estimated by AC voltage and DC voltage (which was used separately to locate the AC and DC transmission line) is used. The improvement of fault location accuracy in this method is shown in Table 9. The waveforms of 1-mode AC voltage from the sending end of the transmission line and the squared wavelet transform coefficient (WTC^2) for AC voltage at scale-1 and DC voltage at scale-2 for LPPGF are shown in Fig. 11.

As can be seen in Fig. 11 (up), the polarity of the first and second voltage traveling waves are same. According to what was presented at the end of section 2.3, it can be concluded that the fault occurred in the second half of the transmission line. Using Fig. 11 (middle) and 11 (down), the fault location can be obtained in two ways using WTC^2 of AC voltage at scale-1 and WTC^2 of DC voltage at scale-2, which is presented below.

$$\text{UsingACvoltagecomponent}: \quad X_f = L - \frac{\nu.(T_{s2} - T_{s1})}{2} = 400 - \frac{2.95 \times 10^5 \times (0.00198 - 0.00073)}{2} = 215.62\ km$$

$$\text{UsingDCvoltagecomponent}: \quad X_f = L - \frac{\nu.(T_{s2} - T_{s1})}{2} = 400 - \frac{2.95 \times 10^5 \times (0.00196 - 0.00072)}{2} = 217.1\ km$$

Table 6
Performance of the fault location method under different fault resistance.

Fault type		Fault	Xact (km)	R_f (Ω)	1st sample	2nd sample	ΔS sample	Polarity of the 1st and 2nd wave	Faulty half	Xcal (km)	Error %	Final Xcal (km)	ABS (total error %)
DC Faults	**SPGF**	**PG**	100	100	33	101	68	Opposite	First	100.30	0.08	**100.30**	**0.08**
			100	200	33	101	68	Opposite	First	100.30	0.08	**100.30**	**0.08**
			100	500	33	101	68	Opposite	First	100.30	0.08	**100.30**	**0.08**
	PPGF	**PNG**	312	100	105	165	60	Same	Second	311.50	-0.13	**311.50**	**0.13**
			312	200	105	165	60	Same	Second	311.50	-0.13	**311.50**	**0.13**
			312	500	105	165	60	Same	Second	311.50	-0.13	**311.50**	**0.13**
AC Faults	**SLGF**	**AG**	270	100	90	180	90	Same	Second	267.25	-0.69	**267.25**	**0.69**
			270	200	90	180	90	Same	Second	267.25	-0.69	**267.25**	**0.69**
			270	500	90	180	90	Same	Second	267.25	-0.69	**267.25**	**0.69**
	LLGF	**ABG**	142	100	46	143	97	Opposite	First	143.08	0.27	**143.08**	**0.27**
			142	200	46	143	97	Opposite	First	143.08	0.27	**143.08**	**0.27**
			142	500	46	143	97	Opposite	First	143.08	0.27	**143.08**	**0.27**
AC/DC intersystem Faults	**LPGF**	**APG**	125	100	41	125	84	Opposite	First	123.90	-0.27	**124.64**	**-0.09**
					43	128	85	Opposite	First	125.38	0.09		
			125	200	41	125	84	Opposite	First	123.90	-0.27	**124.64**	**-0.09**
					43	128	85	Opposite	First	125.38	0.09		
			125	500	41	125	84	Opposite	First	123.90	-0.27	**124.64**	**-0.09**
					43	128	85	Opposite	First	125.38	0.09		
	LLPGF	**ABPG**	255	100	85	185	100	Same	Second	252.50	-0.63	**253.97**	**-0.26**
					85	183	98	Same	Second	255.45	0.11		
			255	200	85	185	100	Same	Second	252.50	-0.63	**253.97**	**-0.26**
					85	183	98	Same	Second	255.45	0.11		
			255	500	85	185	100	Same	Second	252.50	-0.63	**253.97**	**-0.26**
					85	183	98	Same	Second	255.45	0.11		

Table 7
Performance of the fault location method under different noisy environment.

Fault type		Fault	Xact (km)	SNR	1st sample	2nd sample	ΔS sample	Polarity of the 1st and 2nd wave	Faulty half	Xcal (km)	Error %	Final Xcal (km)	ABS (total error %)
DC Faults	**SPGF**	**PG**	152	10 dB	49	153	104	Opposite	First	153.40	0.35	**153.40**	**0.35**
				20 dB	49	153	104	Opposite	First	153.40	0.35	**153.40**	**0.35**
				30 dB	49	153	104	Opposite	First	153.40	0.35	**153.40**	**0.35**
AC Faults	**LLF**	**AC**	278	10 dB	93	283	190	-	-	280.25	0.56	**280.25**	**0.56**
				20 dB	93	283	190	-	-	280.25	0.56	**280.25**	**0.56**
				30 dB	93	283	190	-	-	280.25	0.56	**280.25**	**0.56**
AC/DC intersystem Faults	**LPGF**	**ANG**	364	10 dB	121	145	24	Same	Second	364.60	0.15	**363.13**	**0.22**
					123	149	26	Same	Second	361.65	-0.59		
				20 dB	121	145	24	Same	Second	364.60	0.15	**363.13**	**0.22**
					123	149	26	Same	Second	361.65	-0.59		
				30 dB	121	145	24	Same	Second	364.60	0.15	**363.13**	**0.22**
					123	149	26	Same	Second	361.65	-0.59		

Using Eq. 28, the fault location error for this case using AC and DC voltage components is equal to 0.595% and 0.225%, respectively. The average fault location for this case is 216.36 km and the fault location error is 0.41%. As can be seen, the averaging between the locations estimated by the AC and DC voltage component improves the fault location by the proposed method. Tables 3–5 show other examples for AC, DC and AC/DC intersystem faults location in HPOTLs, respectively. The terms used in Tables 3–9 are as follows:

X_{act}: The actual location of the fault from the sending end of the transmission line

X_{cal}: The calculated location of the fault from the sending end of the transmission line by proposed method

1st sample: The time of the first voltage traveling wave received at the sending end of the transmission line (According to the sampling frequency (100 kHz), each sample is equal to 0.00001 seconds)

2nd sample: The time of the second voltage traveling wave received at the sending end of the transmission line

ΔS sample: The time difference between the first and the second voltage traveling wave received at the sending

Final Xcal (km): average fault location calculated by fault location method for intersystem faults

In Table 5, the data of the first row for each fault is obtained using the WTC^2 of DC voltage at scale-2 and the second row using the WTC^2 of AC voltage at scale-1.

5. Sensitivity analysis

To sensitivity analysis of the proposed fault location method, the effects of various factors have been studied as follows.

A) *Effect of fault resistance*: To inspect the sensitivity of the proposed method to fault resistance, the test system is simulated with a set

Table 8
Performance of the fault location method under different fault angles.

Fault type		Fault	Xact (km)	θ_f	1st sample	2nd sample	ΔS sample	Polarity of the 1st and 2nd wave	Faulty half	Xcal (km)	Error %	Final Xcal (km)	ABS (total error %)
AC Faults	**SLGF**	**AG**	81	0	1677	1731	54	Opposite	First	79.65	-0.34	**79.65**	**0.34**
				30	1837	1891	54	Opposite	First	79.65	-0.34	**79.65**	**0.34**
				45	1927	1981	54	Opposite	First	79.65	-0.34	**79.65**	**0.34**
				60	2007	2061	54	Opposite	First	79.65	-0.34	**79.65**	**0.34**
				90	2177	2231	54	Opposite	First	79.65	-0.34	**79.65**	**0.34**
AC/DC intersystem Faults	**LPGF**	**AN**	280	0	1745	1933	188	-	-	277.30	-0.67	**278.78**	**0.31**
					1745	1935	190	-	-	280.25	0.06		
				30	1905	2093	188	-	-	277.30	-0.67	**278.78**	**0.31**
					1905	2095	190	-	-	280.25	0.06		
				45	1993	2185	192	-	-	283.20	0.80	**280.99**	**0.25**
					1995	2184	189	-	-	278.78	-0.31		
				60	2073	2265	192	-	-	283.20	0.80	**280.99**	**0.25**
					2075	2264	189	-	-	278.78	-0.31		
				90	2245	2433	188	-	-	277.30	-0.67	**278.04**	**0.49**
					2245	2434	189	-	-	278.78	-0.31		
	LLPGF	**ACPG**	332	0	1761	1809	48	Same	Second	329.20	-0.70	**329.20**	**0.70**
					1761	1809	48	Same	Second	329.20	-0.70		
				30	1921	1965	44	Same	Second	335.10	0.78	**332.15**	**0.04**
					1921	1969	48	Same	Second	329.20	-0.70		
				45	2009	2057	48	Same	Second	329.20	-0.70	**329.20**	**0.70**
					2011	2059	48	Same	Second	329.20	-0.70		
				60	2089	2137	48	Same	Second	329.20	-0.70	**329.20**	**0.70**
					2091	2139	48	Same	Second	329.20	-0.70		
				90	2261	2305	44	Same	Second	335.10	0.78	**332.15**	**0.04**
					2261	2309	48	Same	Second	329.20	-0.70		

Table 9
Comparison of different references in the field of fault location in transmission lines

Author's name	Ref.	Publication year	Transmission line's model	Number of circuits	Number of measuring terminals	Sampling frequency	Mean error (%)
L. Xie	[7]	2022	AC	1	Double end data	NA	NA
H. Livani	[8]	2014	DC (underground + overhead)	1	Single end data	200 KHz	0.14
H. Livani	[9]	2010	AC (underground + overhead)	1	Single end data	100KHz	0.5
A. M. Elhaffar	[11]	2008	AC	1	Single and multi-end data	1.25 MHz	0.46
O. Naidu	[14]	2018	AC	1	Double end data	1 MHz	0.02
J. Liu	[16]	2015	DC	1	Double end data	1 MHz	1
Zheng-You He	[17]	2013	DC	1	Single end data	10 MHz	0.17
P. Chen	[18]	2006	DC	1	Multi-end data	1 MHz	0.3
P. Chen	[19]	2008	DC	1	Multi-end data	1 MHz	0.3
A. Swetha	[20]	2011	DC	1	Single end data	80 KHz	1.44
X. Zhang	[21]	2019	DC	1	Double end data	50, 100, 200 KHz	0.44
D. Rezaei	[22]	2022	AC (underground + overhead)	1	Single end data	1 MHz	NA
J. Suonan	[32]	2009	DC	1	Double end data	100 KHz	0.32
M. Ando	[35]	1985	DC	1	Single end data	NA	0.37
Proposed method	**-**	**-**	**Hybrid parallel HVAC/HVDC overhead**	**2**	**Single end data**	**100 KHz**	**0.33**

Table 10
Fault location accuracy in proposed fault location method.

Absolute Fault location error	Mean error (%)	Max error (%)	Max error in transmission line (km)
Absolute Fault location error in DC faults	0.42	0.85	3.4
Absolute Fault location error in AC faults	0.34	0.75	3
Absolute Fault location error in AC/DC faults Based on Vdc1-Scale 2	0.41	0.9	3.6
Absolute Fault location error in AC/DC faults Based on Vac1-Scale 1	0.37	0.88	3.52
Absolute Fault location Cumulative error in AC/DC faults Based on Vdc1-Scale 2 & Vac1-Scale 1	0.25	0.69	2.76
Total mean error in HPOTL	0.33 %		

of different fault resistances up to 500 (Ω). Table 6 gives the performance of the fault location method under different fault. The results presented show that fault resistance has no effect on the performance of the proposed fault location method.

A) *Effect of noise:* To test the robustness of the proposed fault location method under noisy environment, different white Gaussian noises from 10 dB to 30 dB are added to the measured signals and the simulation results are shown in Table 7. It can be inferred that the performance of the proposed fault location method is suitable in noisy environments.

A) *Effect of fault angle*: For the fault angle sensitivity analysis, the test system is simulated with a set of different fault angles on AC voltage waveform (0, 30, 45, 60 and 90). Table 8 gives the performance of the fault location method for some faults under different fault angles. As shown in this table, the proposed method is able to locate the fault with high accuracy in different fault angles.

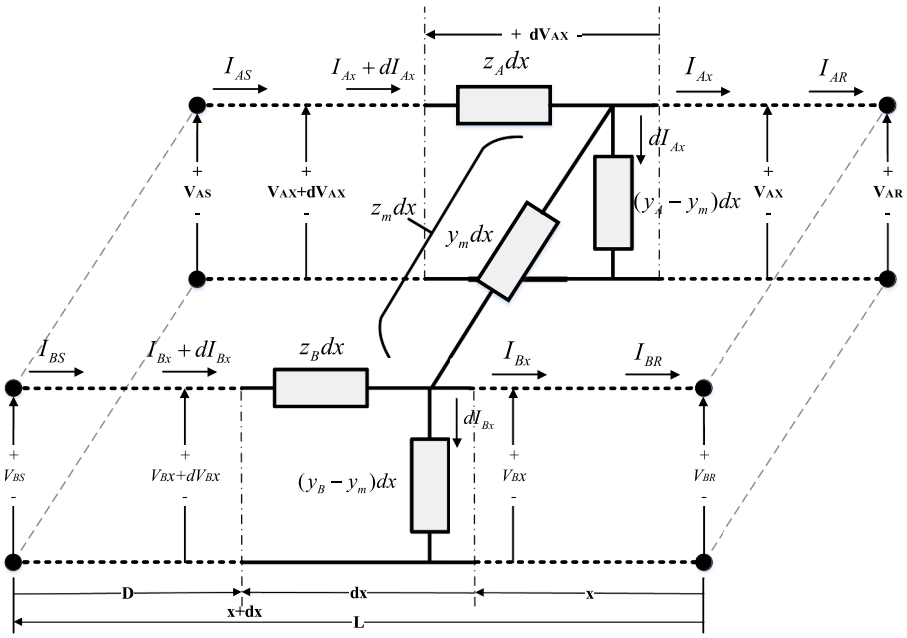

Fig. 12. Differential parameters of mutually coupled parallel transmission lines [38].

6. Discussion and comparison of results

In this section, the obtained results are compared with the results of various references that have been published in the field of traveling wave based fault location in transmission lines. By using indices such as transmission line's model, number of measuring terminals, sampling frequency and mean error of proposed method, it is possible to provide a suitable comparison between the algorithms presented. In Table 9, the papers published in this field of research are compared with one another in different indices presented.

7. Conclusions

In this paper, a single ended traveling wave based fault location method is presented for Hybrid Parallel HVAC/HVDC Overhead Transmission Lines (HPOTLs) on the same tower using Discrete Wavelet Transform (DWT). Since the purpose of this paper is to locate the fault in the HPOTLs, assuming that the fault is detected in the HVAC or/and HVDC transmission line and the faulty lines are identified, the fault location has been done. The classification of faults in the HPOTLs includes AC, DC and AC/DC intersystem faults. The proposed fault location method in this paper is based on the traveling wave's theory. For this purpose, AC and DC transient voltage signals at the sending-end of the transmission line are recorded with sampling frequency of 100 kHz, and then the modal voltage signals are decomposed using the Daubechies4 (Db4-scale 1) wavelet for AC voltage and Haar (Db1-scale 2) wavelet for DC voltage signals. Finally, the location of fault is calculated using squared wavelet transform coefficients (WTC^2) and Bewley-Lattice diagram. Also, for grounded faults, the transmission line faulty-half identification is done by comparing the polarity of the first and second voltage traveling waves observed at the sending end of transmission line. The results obtained from the simulations show the high accuracy of the proposed method for calculating the fault location. Table 9 shows the average and maximum absolute error of fault location in AC, DC and AC/DC intersystem faults. As can be seen in Table 9, using both AC and DC voltage components for intersystem fault location has reduced the average and maximum absolute error of fault location. Also, the sensitivity analysis on the proposed method shows high accuracy, noise immunity, robustness against fault angles and high impedance faults (Table 10).

CRediT authorship contribution statement

Mohammad Fayazi: Conceptualization, Data curation, Formal analysis, Investigation, Methodology, Software, Validation, Writing – original draft. **Mahmood Joorabian:** Project administration, Supervision, Validation, Writing – review & editing. **Alireza Saffarian:** Project administration, Supervision, Validation, Writing – review & editing. **Mehdi Monadi:** Methodology, Resources, Writing – review & editing.

Declaration of Competing Interest

The authors declare that they have no known competing financial interests or personal relationships that could have appeared to influence the work reported in this paper.

Data availability

No data was used for the research described in the article.

Acknowledgements

The authors would like to thank the Shahid Chamran University of Ahvaz for financial support under the grant number SCU.EE1401.63 and SCU.EE1400.373. Also, the authors would like to thank Khuzestan water and power authority (KWPA) and management of the office of applied and research for support for this research.

Appendix: Electromagnetic coupling in parallel transmission lines

The isolated long transmission line is defined in terms of the series impedance and shunt admittance, both expressed per unit of length. It is assumed that the line is completely transposed such that the mutual coupling between phases is exactly balanced and a per-phase representation of the

circuit is permitted [38]. In this case, the voltage and current equations for a single long transmission line in the matrix form is as follows:

$$\begin{bmatrix} V_S \\ I_S \end{bmatrix} = \begin{bmatrix} A & B \\ C & D \end{bmatrix} \begin{bmatrix} V_R \\ I_R \end{bmatrix}, \quad \begin{matrix} A = D = \cosh\gamma L \\ C = Y_c \sinh\gamma L \quad , \quad B = Z_c \sinh\gamma L \end{matrix} \tag{29}$$

When the two long transmission lines are parallel to each other, the transmission lines equations become more complex because, in addition to the parameters of the transmission lines, the mutual impedance and the electromagnetic coupling between the lines must be considered. Fig. 12 shows the differential parameters of two parallel transmission lines that also have electromagnetic coupling. This model is suitable for obtaining voltage and current equations of parallel transmission lines [38].

According to Fig. 12, the voltage and current equations of A and B lines in the matrix form are as follows:

$$\begin{bmatrix} V_{AX} \\ I_{AX} \\ V_{BX} \\ I_{BX} \end{bmatrix} = \underbrace{\begin{bmatrix} A_{AA} & B_{AA} & A_{AB} & B_{AB} \\ C_{AA} & D_{AA} & C_{AB} & D_{AB} \\ A_{BA} & B_{BA} & A_{BB} & B_{BB} \\ C_{BA} & D_{BA} & C_{BB} & D_{BB} \end{bmatrix}}_{M} \begin{bmatrix} V_{AR} \\ I_{AR} \\ V_{BR} \\ I_{BR} \end{bmatrix} \tag{30}$$

Eq. (30) is for any x. In various problems, it is usually tended to calculate voltages and currents on the sending end of transmission line. To do this, we can use the value of L instead of x in the elements of the matrix M in (30). According to Fig. 12, A, B, C and D values in the matrix M in (30) and detailed voltage and current equations of A and B lines are presented as follow:

$$dV_{AX} = (z_A I_{AX} + z_M I_{BX})dx \quad , \quad dV_{Bx} = (z_B I_{BX} + z_M I_{AX})dx \tag{31}$$

$$dI_{AX} = (y_A V_{AX} - y_M V_{BX})dx \quad , \quad dI_{BX} = (y_B V_{BX} - y_M V_{AX})dx \tag{32}$$

Where the two line are coupled by a mutual impedance z_M and by a mutual admittance y_M. Using Eqs. (31) and (32) and then the derivative of the result taken with respect to x to obtain the following form for voltage and current of lines.

$$\begin{bmatrix} \frac{d^2 V_{Ax}}{dx^2} \\ \frac{d^2 V_{Bx}}{dx^2} \end{bmatrix} = \begin{bmatrix} \gamma_{AA}^2 & -\gamma_{AB}^2 \\ -\gamma_{BA}^2 & \gamma_{BB}^2 \end{bmatrix} \begin{bmatrix} V_{AX} \\ V_{BX} \end{bmatrix} \quad , \quad \begin{cases} \gamma_{AA}^2 = z_A y_A - z_M y_M \\ \gamma_{BB}^2 = z_B y_B - z_M y_M \\ \gamma_{AB}^2 = z_A y_M - z_M y_B \\ \gamma_{BA}^2 = z_B y_M - z_M y_A \end{cases} \tag{33}$$

$$\begin{bmatrix} \frac{d^2 I_{Ax}}{dx^2} \\ \frac{d^2 I_{Bx}}{dx^2} \end{bmatrix} = \begin{bmatrix} \gamma_{AA}^2 & -\gamma_{AB}^2 \\ -\gamma_{BA}^2 & \gamma_{BB}^2 \end{bmatrix} \begin{bmatrix} I_{AX} \\ I_{BX} \end{bmatrix} \quad , \quad \begin{cases} \gamma_{AA}^2 = z_A y_A - z_M y_M \\ \gamma_{BB}^2 = z_B y_B - z_M y_M \\ \gamma_{AB}^2 = z_B y_M - z_M y_A \\ \gamma_{BA}^2 = z_A y_M - z_M y_B \end{cases} \tag{34}$$

Taking the Laplace transform and using the initial conditions, we can write (33) and (34) as the following matrix equations.

$$\begin{bmatrix} V_{AX}(s) \\ V_{BX}(s) \end{bmatrix} = \begin{bmatrix} A_{AA}(s) & A_{AB}(s) \\ A_{BA}(s) & A_{BB}(s) \end{bmatrix} \begin{bmatrix} V_{AR} \\ V_{BR} \end{bmatrix} + \begin{bmatrix} B_{AA}(s) & B_{AB}(s) \\ B_{BA}(s) & B_{BB}(s) \end{bmatrix} \begin{bmatrix} I_{AR} \\ I_{BR} \end{bmatrix} \tag{35}$$

$$\begin{bmatrix} I_{AX}(s) \\ I_{BX}(s) \end{bmatrix} = \begin{bmatrix} D_{AA}(s) & D_{AB}(s) \\ D_{BA}(s) & D_{BB}(s) \end{bmatrix} \begin{bmatrix} I_{AR} \\ I_{BR} \end{bmatrix} + \begin{bmatrix} C_{AA}(s) & C_{AB}(s) \\ C_{BA}(s) & C_{BB}(s) \end{bmatrix} \begin{bmatrix} V_{AR} \\ V_{BR} \end{bmatrix} \tag{36}$$

By integrating Eqs. (35) and (36) in the matrix form and transferring to the x domain, (30) is obtained. The matrix elements in Eq. (30) are calculated as follows.

$$A_{AA} = \frac{(\gamma_1^2 - \gamma_{BB}^2)\cosh\gamma_1 x - (\gamma_2^2 - \gamma_{BB}^2)\cosh\gamma_2 x}{\gamma_1^2 - \gamma_2^2} = D_{AA}$$

$$A_{AB} = \frac{\gamma_{AB}^2(\cosh\gamma_1 x - \cosh\gamma_2 x)}{\gamma_1^2 - \gamma_2^2} = D_{BA}$$

$$A_{BA} = \frac{\gamma_{BA}^2(\cosh\gamma_1 x - \cosh\gamma_2 x)}{\gamma_1^2 - \gamma_2^2} = D_{AB}$$

$$A_{BB} = \frac{(\gamma_1^2 - \gamma_{AA}^2)\cosh\gamma_1 x - (\gamma_2^2 - \gamma_{AA}^2)\cosh\gamma_2 x}{\gamma_1^2 - \gamma_2^2} = D_{BB}$$

$$B_{AA} = \frac{\gamma_2\left[(\gamma_1^2 - \gamma_{BB}^2)z_A - \gamma_{AB}^2 z_M\right]\sinh\gamma_1 x - \gamma_1\left[(\gamma_2^2 - \gamma_{BB}^2)z_A - \gamma_{AB}^2 z_M\right]\cosh\gamma_2 x}{\gamma_1\gamma_2(\gamma_1^2 - \gamma_2^2)}$$

$$B_{AB} = \frac{\gamma_2\left[(\gamma_1^2 - \gamma_{BB}^2)z_M - \gamma_{AB}^2 z_B\right]\sinh\gamma_1 x - \gamma_1\left[(\gamma_2^2 - \gamma_{BB}^2)z_M - \gamma_{AB}^2 z_B\right]\cosh\gamma_2 x}{\gamma_1\gamma_2(\gamma_1^2 - \gamma_2^2)}$$

$$B_{BA} = \frac{\gamma_2\left[(\gamma_1^2 - \gamma_{AA}^2)z_M - \gamma_{BA}^2 z_A\right]\sinh\gamma_1 x - \gamma_1\left[(\gamma_2^2 - \gamma_{AA}^2)z_M - \gamma_{BA}^2 z_A\right]\cosh\gamma_2 x}{\gamma_1\gamma_2(\gamma_1^2 - \gamma_2^2)}$$

$$B_{BB} = \frac{\gamma_2\left[\left(\gamma_1^2 - \gamma_{AA}^2\right)z_B - \gamma_{BA}^2 z_M\right]\sinh\gamma_1 x - \gamma_1\left[\left(\gamma_2^2 - \gamma_{AA}^2\right)z_B - \gamma_{BA}^2 z_M\right]\cosh\gamma_2 x}{\gamma_1\gamma_2\left(\gamma_1^2 - \gamma_2^2\right)}$$

$$C_{AA} = \frac{\gamma_2\left[\left(\gamma_1^2 - \gamma_{BB}^2\right)y_A - \gamma_{BA}^2 y_M\right]\sinh\gamma_1 x - \gamma_1\left[\left(\gamma_2^2 - \gamma_{BB}^2\right)y_A - \gamma_{BA}^2 y_M\right]\sinh\gamma_2 x}{\gamma_1\gamma_2\left(\gamma_1^2 - \gamma_2^2\right)}$$

$$C_{AB} = -\frac{\gamma_2\left[\left(\gamma_1^2 - \gamma_{BB}^2\right)y_M - \gamma_{BA}^2 y_B\right]\sinh\gamma_1 x - \gamma_1\left[\left(\gamma_2^2 - \gamma_{BB}^2\right)y_M - \gamma_{BA}^2 y_B\right]\sinh\gamma_2 x}{\gamma_1\gamma_2\left(\gamma_1^2 - \gamma_2^2\right)}$$

$$C_{BA} = -\frac{\gamma_2\left[\left(\gamma_1^2 - \gamma_{AA}^2\right)y_M - \gamma_{AB}^2 y_A\right]\sinh\gamma_1 x - \gamma_1\left[\left(\gamma_2^2 - \gamma_{AA}^2\right)y_M - \gamma_{AB}^2 y_A\right]\sinh\gamma_2 x}{\gamma_1\gamma_2\left(\gamma_1^2 - \gamma_2^2\right)}$$

$$C_{BB} = \frac{\gamma_2\left[\left(\gamma_1^2 - \gamma_{AA}^2\right)y_B - \gamma_{AB}^2 y_M\right]\sinh\gamma_1 x - \gamma_1\left[\left(\gamma_2^2 - \gamma_{AA}^2\right)y_B - \gamma_{AB}^2 y_M\right]\sinh\gamma_2 x}{\gamma_1\gamma_2\left(\gamma_1^2 - \gamma_2^2\right)}$$

$$\gamma_1^2 = \frac{1}{2}\left(\left(z_A y_A + z_B y_B - 2z_M y_M\right) + \sqrt{\left(z_A y_A + z_B y_B - 2z_M y_M\right)^2 - 4\left(z_A z_B - z_M^2\right)\left(y_A y_B - y_M^2\right)}\right)$$

$$\gamma_2^2 = \frac{1}{2}\left(\left(z_A y_A + z_B y_B - 2z_M y_M\right) - \sqrt{\left(z_A y_A + z_B y_B - 2z_M y_M\right)^2 - 4\left(z_A z_B - z_M^2\right)\left(y_A y_B - y_M^2\right)}\right)$$

Solving coupling problems using the classical method increases the complexity and computational load with the number of couplings involved. For example, for the model presented in this paper, a 5-line model (two lines for DC and three lines for AC transmission line) with mutually coupling between them should be considered, and finally the extracted equations are solved and analyzed for the HPOTL model. The equations presented above can be applied to any sequence network in turn. It is well documented in the literature that the coupling between positive and negative sequence networks of lines is very weak. However, coupling between zero sequence networks may be significant and should be the subject of careful analysis [39]. In [38] positive and zero sequences equivalent circuits are provided for the network presented above in the case of line to ground fault, and the equivalent circuit can be used to analyze the fault conditions and obtain the voltage and current equations of sending and receiving end of transmission line in the fault conditions. In this paper, due to the complexity of solving problems related to different faults using analysis of line equations and also high computational load, software simulations have been used to investigate the effect of different faults on mutually coupled transmission lines.

References

[1] P. Ruffing, C. Petino, S. Rüberg, J.C. Garcia, S. Beckler, A. Arnold, Resonance phenomena and dc fault handling during intersystem faults in hybrid ac/dc transmission systems with partial dc cabling. 2018 Power Systems Computation Conference (PSCC), IEEE, 2018, pp. 1–7.

[2] E.V. Larsen, R.A. Walling, C.J. Bridenbaugh, Parallel AC/DC transmission lines steady-state induction issues, IEEE Trans. Power Delivery 4 (1) (1989) 667–674.

[3] M. Kizilcay, A. Agdemir, M. Losing, Interaction of a HVDC system with 400-kV AC systems on the same tower, in: International Conference on Power System Transient in Kyoto, Japan June, 2009, pp. 3–6.

[4] J. J. Hu and B. Bisewski, "Evaluation of coupling between dc and ac transmission lines on the same right-of-way: parametric analysis and mitigation methods," in *MIPSYCON*, 2011.

[5] "IEEE draft guide for determining fault location on AC transmission and distribution lines," *IEEE PC37.114/D9, July 2014,* pp. 1-72, 2014.

[6] M. Abasi, A. Rohani, F. Hatami, M. Joorabian, G.B. Gharehpetian, Fault location determination in three-terminal transmission lines connected to industrial microgrids without requiring fault classification data and independent of line parameters, Int. J. Electric. Power & Energy Syst. 131 (2021), 107044.

[7] L. Xie, et al., A novel fault location method for hybrid lines based on traveling wave, Int. J. Electric. Power & Energy Syst. 141 (2022), 108102, 2022/10/01/.

[8] H. Livani, C.Y. Evrenosoglu, A single-ended fault location method for segmented HVDC transmission line, Electr. Power Syst. Res. 107 (2014) 190–198.

[9] H. Livani, C.Y. Evrenosoglu, A traveling wave based single-ended fault location algorithm using DWT for overhead lines combined with underground cables. IEEE PES General Meeting, IEEE, 2010, pp. 1–6.

[10] D. Tzelepis, et al., Voltage and current measuring technologies for high voltage direct current supergrids: a technology review identifying the options for protection, fault location and automation applications, IEEE Access 8 (2020) 203398–203428.

[11] A. M. Elhaffar, "Power transmission line fault location based on current traveling waves," 2008.

[12] F.H. Magnago, A. Abur, Fault location using wavelets, IEEE Trans. Power Delivery 13 (4) (1998) 1475–1480.

[13] M. Gilany, E. Eldin, D. Ibrahim, Travelling wave-based fault location scheme for multi-end aged underground cable system, Int. J. Power and Energy Syst. 28 (2) (2008) 160.

[14] O. Naidu, A.K. Pradhan, A traveling wave-based fault location method using unsynchronized current measurements, IEEE Trans. Power Delivery 34 (2) (2018) 505–513.

[15] L. de Andrade, M.T.P. de Leao, Fault location for transmission lines using wavelet, IEEE Latin America Trans. 12 (6) (2014) 1043–1048.

[16] J. Liu, J. Duan, H. Lu, Y. Sun, Fault location method based on EEMD and traveling-wave speed characteristics for HVDC transmission lines, Journal of power and Energy Engineering 3 (4) (2015) 106–113.

[17] Z.-Y. He, K. Liao, X.-P. Li, S. Lin, J.-W. Yang, R.-K. Mai, Natural frequency-based line fault location in HVDC lines, IEEE Trans. Power Delivery 29 (2) (2013) 851–859.

[18] P. Chen, B. Xu, J. Li, A traveling wave based fault locating system for HVDC transmission lines. 2006 International Conference On Power System Technology, IEEE, 2006, pp. 1–4.

[19] P. Chen, B. Xu, J. Li, Y. Ge, Modern travelling wave based fault location techniques for HVDC transmission lines, Trans. Tianjin University 14 (2) (2008) 139–143.

[20] A. Swetha, P.K. Murthy, N. Sujatha, Y. Kiran, A novel technique for the location of fault on a HVDC transmission line, J. Eng. Appl. Sci 6 (11) (2011) 62–67.

[21] X. Zhang, N. Tai, X. Zheng, W. Huang, Wavelet-based EMTR method for fault location of VSC-HVDC transmission lines, The J. Eng. 2019 (16) (2019) 961–966.

[22] D. Rezaei, M. Gholipour, F. Parvaresh, A single-ended traveling-wave-based fault location for a hybrid transmission line using detected arrival times and TW′ s polarity, Electr. Power Syst. Res. 210 (2022), 108058.

[23] A. A. Ashagire, "Study on conversion of existing HVAC lines to hybrid HVAC/HVDC transmission line to increase transmission capacity and efficiency," Addis Ababa Institute of Technology School of Electrical and Computer Engineering, 2015.

[24] A. Novitskiy and D. Westermann, "Some aspects of steady state simulations of AC/DC hybrid transmission lines," in *2017 IEEE International Conference on Environment and Electrical Engineering and 2017 IEEE Industrial and Commercial Power Systems Europe (EEEIC /I&CPS Europe)*, 2017, pp. 1-4.

[25] C. Petino, P. Ruffing, and A. Schnettler, "Intersystem fault clearing in hybrid AC/DC power systems with full bridge modular multilevel converters," 2017.

[26] G. Ebner, D. Döring, F. Schettler, K. Würflinger, M. Zeller, Fault handling at hybrid high-voltage AC/DC transmission lines with VSC converters, IEEE Trans. Power Delivery 33 (2) (2018) 901–908.

[27] X.-h. Li, Z.-p. Liang, Z.-x. Cai, Induced components in HVDC transmission lines caused by same-tower AC system faults. 2018 International Conference on Power System Technology (POWERCON), IEEE, 2018, pp. 2791–2798.

[28] T. Nazarcik and V. Muzik, "Modelling of the mutual influence of the parallel AC/DC circuits on the hybrid power transmission line," in *2018 IEEE Conference of Russian Young Researchers in Electrical and Electronic Engineering (EIConRus)*, 2018, pp. 731-736.

[29] J. Prommetta, J. Schindler, J. Jaeger, T. Keil, C. Butterer, AC-protection in the context of AC/Dc-hybrid lines. 2019 IEEE 8th International Conference on Advanced Power System Automation and Protection (APAP), IEEE, 2019, pp. 1854–1858.

[30] X. Dong, E. Guan, L. Jing, H. Wang, S. Mirsaeidi, Simulation and analysis of cascading faults in hybrid AC/DC power grids, Int. J. Electric. Power & Energy Syst. 115 (2020), 105492.

[31] J. Prommetta, J. Schindler, J. Jaeger, T. Keil, C. Butterer, G. Ebner, Protection coordination of AC/DC intersystem faults in hybrid transmission grids, IEEE Trans. Power Delivery (2020).
[32] J. Suonan, S. Gao, G. Song, Z. Jiao, X. Kang, A novel fault-location method for HVDC transmission lines, IEEE Trans. Power Delivery 25 (2) (2009) 1203–1209.
[33] K. De Kerf, et al., Wavelet-based protection strategy for DC faults in multi-terminal VSC HVDC systems, IET Generation, Trans. Distribution 5 (4) (2011) 496–503.
[34] C.H. Kim, R. Aggarwal, Wavelet transforms in power systems. Part 1: General introduction to the wavelet transforms, Power Eng. J. 14 (2) (2000) 81–87.
[35] M. Ando, E. Schweitzer, R. Baker, Development and field-data evaluation of single-end fault locator for two-terminal HVDV transmission lines-part 2: Algorithm and evaluation, IEEE Trans. Power Apparatus and Syst. (12) (1985) 3531–3537.
[36] A. Greenwood, "Electrical transients in power systems," 1991.
[37] M. Szechtman, et al., The CIGRE HVDC benchmark model-a new proposal with revised parameters, Electra 157 (2) (1994) 61–66.
[38] P.M. Anderson, C. Henville, R. Rifaat, B. Johnson, S. Meliopoulos, Power System Protection, John Wiley & Sons, 2022.
[39] T. Arro and O. Silavwe, "Coupling of transients in HVDC lines to adjacent HVAC lines and its impact on the AC line protection," 2007.